JACS
JOURNAL OF THE AMERICAN CHEMICAL SOCIETY
Article
Cite This: J. Am. Chem. Soc. 2018, 140, 3461−3466
pubs.acs.org/JACS

Controlled Gas Uptake in Metal−Organic Frameworks with Record Ammonia Sorption

Adam J. Rieth and Mircea Dincă*

Department of Chemistry, Massachusetts Institute of Technology, 77 Massachusetts Avenue, Cambridge, Massachusetts 02139, United States

Supporting Information

ABSTRACT: Ammonia is a vital commodity in our food supply chain, but its toxicity and corrosiveness require advanced protection and mitigation. These needs are not met efficiently by current materials, which suffer from either low capacity or low affinity for NH_3. Here, we report that a series of microporous triazolate metal−organic frameworks containing open metal sites exhibit record static and dynamic ammonia capacities. Under equilibrium conditions at 1 bar, the materials adsorb up to 19.79 mmol NH_3 g^{-1}, more than twice the capacity of activated carbon, the industry standard. Under conditions relevant to personal protection equipment, capacities reach 8.56 mmol g^{-1}, 27% greater than the previous best material. Structure−function relationships and kinetic analyses of NH_3 uptake in isostructural micro- and mesoporous materials made from Co, Ni, and Cu reveal stability trends that are in line with the water substitution rates in simple metal−aquo complexes. Altogether, these results provide clear, intuitive descriptors that govern the static and dynamic uptake, kinetics, and stability of MOF sorbents for strongly interacting gases.

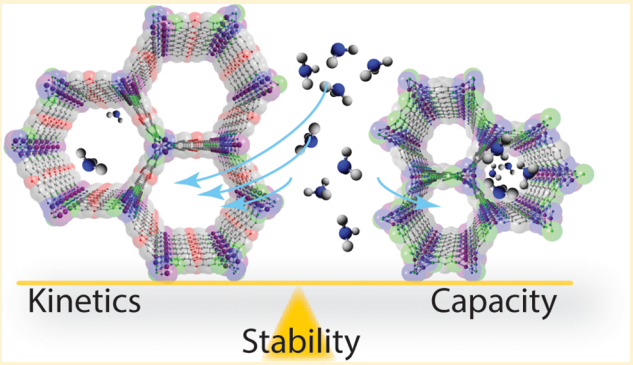

INTRODUCTION

As an irreplaceable feedstock for global agriculture and industry,[1] ammonia is produced at a rate of 140 million metric tons per year, making it among the largest volume chemicals on the planet.[2] Although critical to our food supply and economy, NH_3 is a highly toxic gas even in small concentrations. Therefore, sorbents capable of removing trace NH_3 are of interest for industrial air remediation, personal protective equipment, as well as separation of NH_3 from N_2 and H_2.[3,4] For these varied applications, uptake at low NH_3 concentrations is required, yet the current industrial standard sorbents, activated carbons, suffer from relatively low affinity as well as limited capacity for NH_3.[5,6] More fundamentally, the heterogeneity of pore sizes in carbons has prevented systematic studies of ammonia sorption in microporous materials, which are crucial for improved adsorbent designs.[7]

To address this need, recent efforts have focused on developing sorbents with Lewis or Brønsted acidic active sites that impart higher affinity for the basic NH_3 molecule.[8,9] Metal−organic frameworks (MOFs) with coordinatively unsaturated, Lewis acidic open metal sites such as Cu_3(trimesate)$_2$ (HKUST-1), Mg_2(2,5-dihydroxybenzenedicarboxylate) (Mg-MOF-74), and Co(isonicotinic acid)$_2$ have emerged as superlative dry NH_3 adsorbents. However, their performance almost invariably suffers upon repeated exposure to NH_3, and, more critically, they often degrade upon exposure to water vapor.[10−12] Porous polymers with a high density of Brønsted acid sites also demonstrate superior NH_3 sorption,[9,13] their stable all-carbon backbone offering distinct advantages for performance under humid conditions. However, the heterogeneous pore size distribution in these porous organic polymers impedes studies of pore size effects on sorption kinetics.[13] Further, the interpenetrated nature of the porous polymers leads to a highly tortuous pore network with small windows, which substantially retards gas uptake.[9] Indeed, although a high maximum NH_3 capacity is desirable, increasing the uptake often comes at the expense of slower sorption kinetics. For instance, nonporous $MgCl_2$ has the greatest capacity for ammonia of any known material, but slow kinetics as well as a large volume expansion upon NH_3 uptake limit its utility in many applications.[14] Despite its obvious importance, the kinetics of ammonia sorption in porous materials is seldom investigated. Reports of sorbent performance overwhelmingly focus on uptake capacity with no mention of adsorption kinetics or, at best, only indirect investigations through the analysis of gas breakthrough experiments.[13,15]

Recently, we reported a series of particularly robust MOFs, M_2Cl_2(BTDD) (M = Mn, Co, Ni, Cu; BTDD = bis(1*H*-1,2,3-triazolo[4,5-*b*],[4′,5′-*i*])dibenzo[1,4]dioxin),[16,17] which feature large hexagonal mesoporous channels with a diameter of 2.3 nm lined with chains of Lewis acidic metals that exhibit open coordination sites (Figure 1). These materials were the first examples of MOFs that were stable to repeated sorption and

Received: January 9, 2018
Published: February 9, 2018

DOI: 10.1021/jacs.8b00313
J. Am. Chem. Soc. 2018, 140, 3461−3466

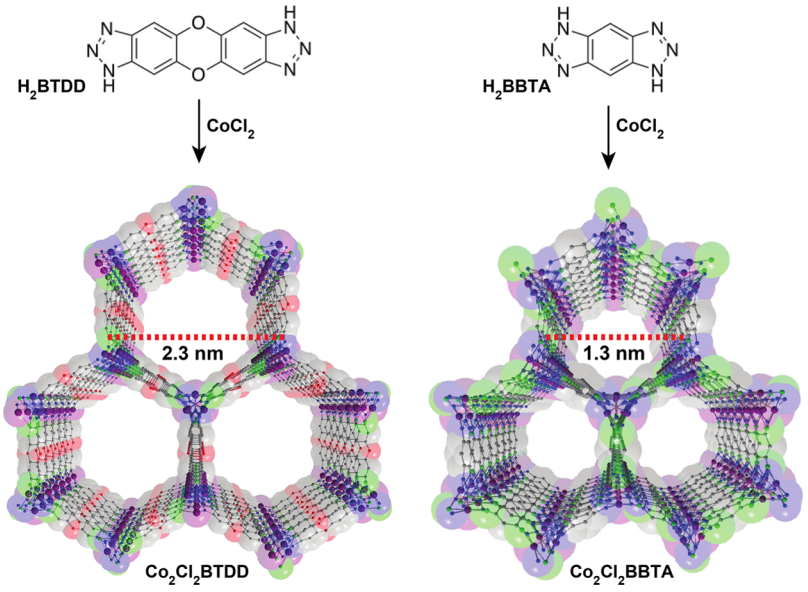

Figure 1. Synthesis and structure of Co_2Cl_2BTDD (left) and Co_2Cl_2BBTA (right). C, gray; O, red; N, blue; Cl, green; Co, purple. Hydrogen atoms have been omitted for clarity.

desorption of ammonia. Their extreme stability to corrosive gases was further highlighted by repeated exposure to chlorine and bromine gas, which can also be stored reversibly in these materials over multiple cycles.[16,18] Here, we utilize these materials and their smaller-pore isoreticular analogues, M_2Cl_2BBTA (M = Co, Ni, Cu; BBTA = 1*H*,5*H*-benzo(1,2-*d*),(4,5-*d*′)bistriazole),[19,20] as a ready-made platform for interrogating the effects of modifying the pore size and active site density on the total uptake and the kinetics of ammonia sorption. We show that the higher capacity for ammonia in the smaller-pore materials cannot be accounted for simply by the increase in the density of open metal sites. Instead, cooperative proximity effects likely lead to the anomalous observed increase in ammonia saturation uptake for M_2Cl_2BBTA. Using Infra-SORP,[21−23] a recently developed calorimetric technique, we further draw correlations between pore size and sorption kinetics. Finally, we show that MOF stability to ammonia or water, an oft-empirical parameter of fundamental and practical importance, correlates directly with the water exchange rates in homoleptic metal−aquo complexes, a fundamental property established decades ago[24] that will serve as an easy guide for new MOF design in the future.

RESULTS AND DISCUSSION

Ammonia sorption experiments for activated samples of M_2Cl_2BBTA (M = Co, Ni, Cu) at 298 K revealed type I isotherms, with steep uptakes at low absolute pressure (Figure 2). The total NH_3 uptakes at 1 bar were 17.95, 14.68, and 19.79 mmol NH_3 g^{-1} for the Co, Ni, and Cu analogues, respectively. As compared to the larger pore BTDD materials, the uptakes observed for BBTA materials are considerably higher,[16] positioning Cu_2Cl_2BBTA as the material with the highest NH_3 uptake among all MOFs. Intriguingly, the increase in gravimetric capacity in going from M_2Cl_2BTDD to the smaller pore M_2Cl_2BBTA is greater than what would be expected from simply increasing the density of active open metal sites. For instance, the equilibrium uptake of 2.72 molecules of NH_3 per Co atom at 1 bar and 298 K in mesoporous Co_2Cl_2BTDD[16] increases to 3.20 molecules of NH_3 per Co atom in

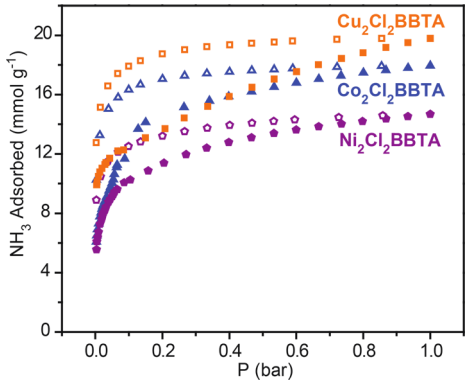

Figure 2. NH_3 adsorption (closed symbols) and desorption (open symbols) of activated samples of Co_2Cl_2BBTA (blue triangles), Ni_2Cl_2BBTA (purple pentagons), and Cu_2Cl_2BBTA (orange squares) at 298 K.

microporous Co_2Cl_2BBTA. We attribute this anomalous increase in ammonia density to the shorter distance between neighboring chains of metal-bound NH_3 molecules in Co_2Cl_2BBTA. This may allow for increased hydrogen-bonding interactions between the first, metal-bound NH_3 molecules and additional NH_3 adsorbed in the pore to an extent that is not available in the larger-pore M_2Cl_2BTDD series. In support of this hypothesis, we note that a similar confinement effect is operative for NH_3 uptake in microporous zeolites.[25]

After exposure to NH_3 at 1 bar and 298 K, Ni_2Cl_2BBTA retains its crystallinity and porosity (Figures S4.1 and S5.2), whereas Cu_2Cl_2BBTA becomes amorphous and nonporous (Figures S4.2 and S5.3), both in line with the behavior observed for the respective larger pore analogues (for Cu_2Cl_2BTDD,[26] Figures S3.2, S4.3, and S5.4).[16] By contrast, powder X-ray diffraction (PXRD) measurements indicate that Co_2Cl_2BBTA, unlike its larger pore analogue, loses much of its crystallinity upon exposure to 1 bar ammonia (Figure S4.4). This also leads to increased hysteresis during desorption (Figure 2) and substantially reduced Brunauer−Emmett−Teller (BET) surface area (Figure S5.5 and Table S5.1).

DOI: 10.1021/jacs.8b00313
J. Am. Chem. Soc. 2018, 140, 3461−3466

Although Co_2Cl_2BBTA collapses upon exposure to 1 bar NH_3, it remains stable and retains its porosity at 1 mbar NH_3, conditions that are more relevant for personal protection equipment (Figures S4.4 and S5.5). Furthermore, NH_3 cycling experiments revealed that, despite its collapse at higher ammonia pressure, Co_2Cl_2BBTA retains a substantial uptake upon cycling with reactivation at 200 °C. These results mirror those observed for mesoporous Mn_2Cl_2BTDD (Figure S3.1)[16] and are in line with other studies that have shown that a decrease in surface area does not predict a decline in the ammonia uptake; rather, the interaction strength between bonding sites and ammonia is a more important predictor of ammonia uptake.[9,27] Although the total surface area decreases, the open metal sites that strongly bind ammonia evidently remain accessible.

The different stability observed for Co_2Cl_2BBTA and Co_2Cl_2BTDD under identical conditions was intriguing because in the vast majority of MOFs where the primary coordination sphere of the metal is conserved, as here, it is the larger pore material that undergoes pore collapse more readily.[19] To investigate this anomalous behavior, we measured a series of variable temperature ammonia isotherms for the larger pore Co_2Cl_2BTDD. More pronounced hystereses became evident as the isotherm temperature dropped below 298 K, and at 263 K we observed a hysteresis in Co_2Cl_2BTDD similar to that in Co_2Cl_2BBTA (Figure 3). As with the small

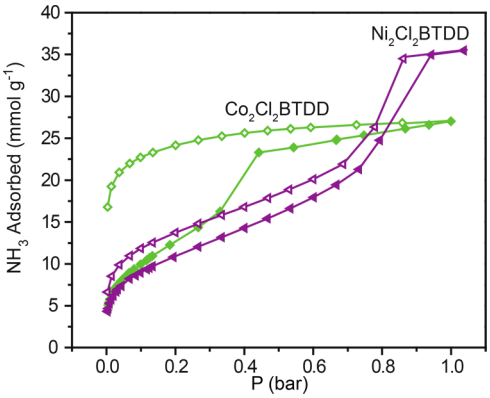

Figure 3. NH_3 adsorption (closed symbols) and desorption (open symbols) of activated samples of Co_2Cl_2BTDD (green diamonds) and Ni_2Cl_2BTDD (purple triangles) at 263 K.

pore analogue, this lower temperature NH_3 isotherm also led to partial structural collapse and decreased crystallinity (Figure S4.5). These experiments showed that pore collapse and hysteresis are closely correlated with the local concentration of ammonia in the pore. The cobalt frameworks are stable when ammonia uptake is limited at and around the open metal sites in a layer/cluster mechanism, but if the pores of these materials start filling with ammonia, which begins to occur at room temperature for the small-pore analogue and at lower temperature for the large-pore material, the crystallinity suffers. With Ni_2Cl_2BTDD, ammonia sorption remains quasi-reversible even at 263 K, although the isotherm profile changes relative to the 298 K isotherm, with the 298 K capacity reached at only 0.4 bar, followed by a pronounced step increase and saturation at 35 mmol g^{-1} at 1 bar (Figure 3). The increase in uptake followed by saturation is characteristic of pore-filling behavior, observed previously in these systems for water adsorption.[17] Importantly, Ni_2Cl_2BTDD retains its crystallinity and high surface area even after pore filling (Figures S4.6 and S5.6) and represents, to our knowledge, the first example of reversible ammonia pore-filling behavior in a MOF, of potential interest for adsorption heat pumps.[28]

Simple Kinetic Descriptors Define MOF Stability toward Polar Coordinating Molecules. Calorimetric measurements and theoretical calculations have shown that porous phases of MOFs are almost universally metastable, that is, uphill in energy with respect to their dense phases.[29,30] Finding the more stable structures in this class has largely been empirical, but, as with any material, stabilization of a metastable porous MOF phase relative to the dense phase can only be kinetic. It must involve raising the reaction coordinate energy barrier between the two phases, either by decreasing the energy of the porous phase or by increasing the transition state energy. The former is more intuitive: extensive previous work has shown that increasing the metal−ligand bond strength, generally the weakest link in MOF structures, results in enhanced stability toward polar analytes, for example, water and ammonia, a result of lowering the energy of the porous frameworks.[31−34] Similarly, the triazolate frameworks investigated here already exhibit enhanced stability over their carboxylate containing counterparts such as MOF-74.[35,36] Here, we further posit that the stability trend within this family of triazolate MOFs follows the kinetic metal−aquo substitution rate, an effect of the transition state energy. The Ni^{2+} materials are most stable toward ammonia: the small-pore Ni_2Cl_2BBTA framework is the only one to retain its surface area after exposure to 1 bar NH_3, and the large-pore Ni_2Cl_2BTDD withstands pore filling with NH_3. The Co^{2+} materials both withstand layer-cluster ammonia binding, but not pore filling, whereas the Cu^{2+} and Mn^{2+} materials degrade even at low concentrations of ammonia. This stability trend is in line with the experimentally observed kinetic metal−aquo substitution rate. Ni^{2+} is 2 orders of magnitude more kinetically inert than Co^{2+}, which, in turn, is approximately 2 orders of magnitude more kinetically inert than either Mn^{2+} or Cu^{2+}.[24] We note that kinetic stability has also been invoked to explain the exceptional robustness of the carboxylate-based Cr^{3+}-containing MIL-101.[37,38] Notably, in the MIL-53 and -47 family of isostructural frameworks, cation inertness is a more relevant predictor of stability: chemical robustness decreases in the order $Cr^{3+} > Al^{3+} > V^{4+}$, in line with the water substitution rates in the respective aquo complexes, but diverging from the thermodynamic trend in metal−oxygen bond strength.[39] Further, even partial replacement of Mg^{2+} in Mg-MOF-74 with more inert Ni^{2+} ions significantly enhances the stability of the Mg material.[40] Although incorporation of kinetically inert metals into MOFs can be challenging synthetically,[41,42] future efforts in this direction can provide a route toward enhancing chemical robustness.

Pore Size Effects on Breakthrough Performance and Kinetics. The small- and large-pore cobalt frameworks contain identical, stable, strongly adsorptive active sites, which are regularly spaced through one-dimensional pores of varying diameters, providing an ideal platform to investigate the effects of pore size on NH_3 breakthrough performance as well as kinetics. Dynamic breakthrough measurements at 1000 ppm of NH_3 revealed that Co_2Cl_2BBTA has a record dry capacity (uptake until 1000 ppm is reached) of 8.56 mmol g^{-1}, 27% higher than the state-of-the-art HKUST-1,[43] while the larger-pore Co_2Cl_2BTDD has a capacity of 4.78 mmol g^{-1} (Figure 4A, Table 1). These breakthrough capacities are equal to 1.48

DOI: 10.1021/jacs.8b00313
J. Am. Chem. Soc. 2018, 140, 3461−3466

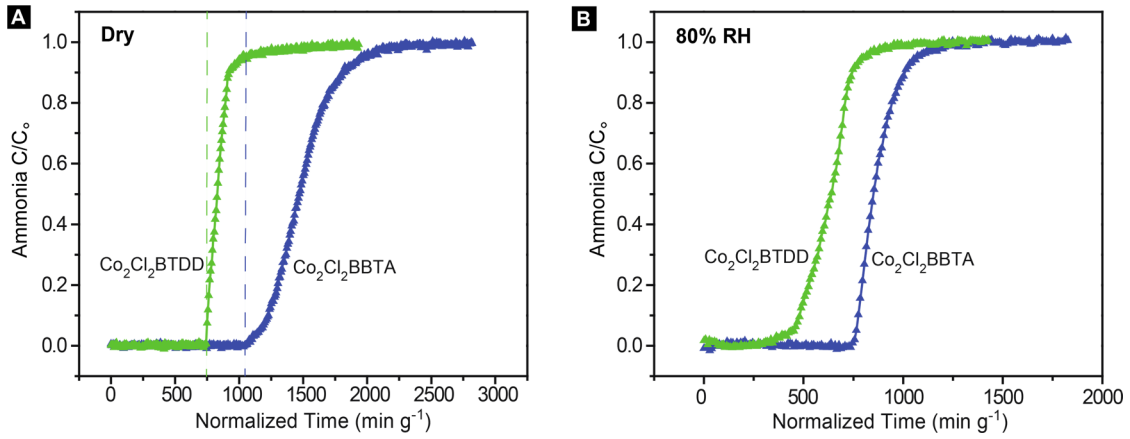

Figure 4. Ammonia breakthrough curves for large-pore Co_2Cl_2BTDD (green) and small-pore Co_2Cl_2BBTA (blue) under (A) dry (0% RH) and (B) wet (80% RH) conditions. Dashed lines in (A) indicate 1 molecule of NH_3 adsorbed per open coordination site. The challenge concentration C_o was 1000 ppm with a flow rate of 140 mL min^{-1}.

Table 1. Saturation NH_3 Breakthrough Capacities at 1000 ppm in mmol g^{-1} for Co_2Cl_2BTDD, Co_2Cl_2BBTA, and Cu_2Cl_2BBTA (Figure S3.3)

	dry (0% RH)	wet (80% RH)
Co_2Cl_2BTDD	4.78	3.38
Co_2Cl_2BBTA	8.56	4.36
Cu_2Cl_2BBTA	7.52	5.73

molecules of NH_3 per Co atom for the small-pore material and 1.08 molecules per open Co site for the large-pore material. Interestingly, the breakthrough criterion for ammonia (5 ppm) is reached after the small-pore material has adsorbed 6.24 mmol g^{-1} NH_3 and the large-pore MOF has adsorbed 4.42 mmol g^{-1} NH_3, corresponding to 1.08 and 1.00 molecules of ammonia per open metal site, respectively. These results demonstrate that increasing the density of open metal sites results in a linear increase in the breakthrough performance, while the saturation capacity is further enhanced in the small pore material, in line with the proximity effects observed in the static isotherms discussed above. In the dry breakthrough curves, the NH_3 concentration remains at the baseline until all metal sites have been filled, and then the downstream concentration begins to rise (Figure 4A). The steep increase in downstream NH_3 concentration for the large-pore material further evidences weaker secondary interactions as compared to the shallow sigmoidal rise in concentration for the small-pore material.

Expectedly, NH_3 breakthrough measurements performed at 80% relative humidity (RH) revealed that both small-pore Co_2Cl_2BBTA and large-pore Co_2Cl_2BTDD are affected by moisture (Figure 4B, Table 1). Co_2Cl_2BBTA retains a saturation capacity of 4.36 mol kg^{-1}, whereas Co_2Cl_2BTDD has a humid saturation capacity of 3.38 mol kg^{-1}. These values correspond to 0.76 and 0.77 NH_3 molecules per open metal site, respectively, a decrease from the dry case that is clearly due to competitive adsorption with water.[17] These humid breakthrough capacities remain superior to conventional porous materials such as zeolites and activated carbons,[5] and show promise for air purification applications.

The breakthrough experiments demonstrate that the kinetics of NH_3 uptake, obviously vital for both personal protection and gas separations applications,[44] are not easily predicted by static isotherm measurements, although many studies of NH_3 adsorbents focus solely on capacity. We interrogated the

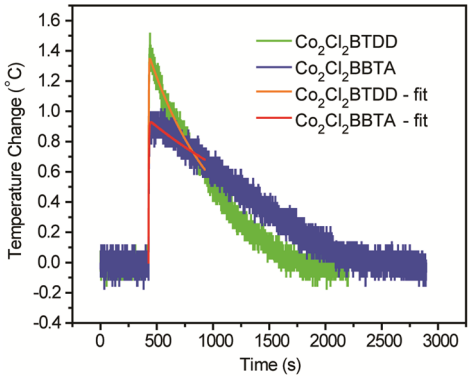

Figure 5. "InfraSORP" heat flux upon introduction of 1000 ppm ammonia in nitrogen at a flow rate of 140 mL min^{-1} to samples of large-pore Co_2Cl_2BTDD (green) and small-pore Co_2Cl_2BBTA (blue).

kinetics of NH_3 uptake in Co_2Cl_2BBTA and Co_2Cl_2BTDD using InfraSORP, an optical calorimetric method.[21−23] Measurements revealed that the large-pore material has significantly more rapid ammonia uptake (Figure 5). Fitting of the initial 500 s of calorimetric data to two exponentials according to the equation: $T = T_o((1 - e^{-k_1 t}) - (1 - e^{-k_2 t}))$ showed first-order rate constants, k_1, for NH_3 uptake of 0.42 and 0.28 s^{-1} for the large-pore and the small-pore Co frameworks, respectively (Figures S7.1 and S7.2). This is not surprising: NH_3 molecules are able to more swiftly reach all open Co sites in the larger pores of Co_2Cl_2BTDD.

The optical calorimetric method assumes that the two materials have equivalent heats of adsorption for ammonia and similar heat capacities. To test these assumptions, the areas under the kinetics curves were integrated and multiplied by the sample masses, providing an estimate for the energy absorbed into the materials (Figures S7.3−S7.6), which should correlate with the amount of ammonia adsorbed, as confirmed previously in other systems.[21−23] The ratio of heat transferred to the small pore versus the large pore as determined by InfraSORP was 1.49, in excellent agreement with the ratio of 1.48 for equilibrium NH_3 capacities at 1 mbar determined from low pressure NH_3 isotherms (Figure S3.4), validating the applicability of the InfraSORP method for ammonia.

The kinetic data provide predictive power when combined with relevant models for gas diffusion, such as the Knudsen

DOI: 10.1021/jacs.8b00313
J. Am. Chem. Soc. 2018, 140, 3461−3466

model.[45] The latter applies when the mean free path of the analyte molecule is larger than the pore diameter of the sorbent.[45] Here, the mean free path for NH_3 with a kinetic diameter of 0.326 nm at 25 °C and 1 bar is 871 Å, indeed much greater than either of the pore diameters of our materials, 13 and 23 Å. In these scenarios, the flux from gas-phase ammonia to an intrapore adsorption site can be approximated as that for a circular tube with rigid, nonadsorbing walls, and is given by

$$F = \frac{1}{3}\sqrt{\frac{8RT}{\pi M}}\frac{d\varepsilon}{L\tau}$$

where M is the molecular weight of NH_3, R is the gas constant, T is the temperature, d is the pore diameter, ε is the void fraction, L is the length of the path from the gas phase to the inner adsorption site, and τ is the tortuosity. Because M, R, T, and τ are identical in both MOFs, the flux ratio for large pore (L) to small pore (S) materials is

$$\frac{F_L}{F_S} = \frac{d_L\varepsilon_L L_S}{d_S\varepsilon_S L_L}$$

Using pore diameters determined by Barrett–Joyner–Halenda[46,47] theory of 13 and 23 Å (Figure S5.1), and crystallographic void fractions of 0.4403[20] and 0.6266[16] for Co_2Cl_2BBTA and Co_2Cl_2BTDD, respectively, we would expect the ratio of uptake rates (i.e., flux ratio) between the large-pore and small-pore materials to be $2.5L_S/L_L$. The ratio L_S/L_L is difficult to quantify because the average diffusional distance to each active site depends on particle length and aspect ratio, as well as differences in active site density. As such, L_S/L_L was estimated by scanning electron microscopy (Figures S6.1 and S6.2), which showed that crystallites of the small pore material were on average one-half the size of those observed for the large pore MOF, allowing us to approximate L_S/L_L as ∼0.5. Overall, the expected flux ratio F_L/F_S was thus expected to be approximately 1.25, in good agreement with the experimentally determined ratio of rate constants of 1.5.

Altogether, the kinetic data show that the Knudsen model serves as a reasonable baseline for understanding and predicting the effects of modifying the pore size and the crystallite size on the speed of gas uptake in MOFs, even when the analytes are strongly interacting gases, and that decreasing particle size can mitigate the slower uptake kinetics resulting from reducing the pore size. Future research aimed at uncovering the kinetics of gas sorption in MOFs in finer detail will further aid prediction of material suitability for varied applications including personal protective equipment, separations, and heat pumps.

CONCLUSIONS

Stable triazolate frameworks containing open metal sites provide a unique platform for interrogating coordinating and corrosive gas sorption. Because of their higher density of open metal sites, the smaller-pore BBTA materials have significantly greater capacities than their larger-pore counterparts, with Cu_2Cl_2BBTA exhibiting the greatest static uptake at 1 bar and 298 K of any MOF or porous organic polymer. Additionally, increasing the density of open metal sites results in a linear increase in breakthrough performance, as the breakthrough criterion for NH_3, 5 ppm, is reached after one molecule of ammonia is adsorbed per open metal site in both small-pore Co_2Cl_2BBTA and large-pore Co_2Cl_2BTDD. Increasing the density of open metal sites results in a record dry dynamic ammonia capacity for Co_2Cl_2BBTA at 1000 ppm of 8.56 mmol g^{-1}, exceeding that of the state-of-the-art HKUST-1 by 27%. Decreasing the pore size from 23 to 13 Å results in slower sorption kinetics, although this effect can be mitigated by synthesizing smaller MOF particles. Kinetic analyses correlate with the Knudsen flux model, demonstrating that this theoretical framework serves as a good baseline to predict the effects of modifying the pore size as well as the particle size on sorbent kinetic performance. Further, the stability trend of the isoreticular frameworks substituted with various metal ions follows the metal–aquo substitution rate, with the large-pore framework formed with the most inert metal, Ni_2Cl_2BTDD, able to withstand pore filling with NH_3 at low temperature. This work provides a clear path toward designer sorbents by controlling the uptake, kinetics, and stability of the active materials.

ASSOCIATED CONTENT

Supporting Information

The Supporting Information is available free of charge on the ACS Publications website at DOI: 10.1021/jacs.8b00313.

Synthetic details, physical methods, InfraSORP curve fitting methods, and Figures S3.1–S7.6 (PDF)

AUTHOR INFORMATION

Corresponding Author

*mdinca@mit.edu

ORCID

Mircea Dincă: 0000-0002-1262-1264

Notes

The authors declare the following competing financial interest(s): AJR and MD are listed as inventors on a patent pertaining to the materials used in this work.

ACKNOWLEDGMENTS

This work was supported by the Tata Center for Technology and Design. Fundamental studies of metal-small molecule interactions in MOFs were supported by a National Science Foundation CAREER Award to M.D. (DMR-1452612). We thank Dr. R. Day for assistance with acquiring the SEM images.

REFERENCES

(1) Zhang, X.; Davidson, E. A.; Mauzerall, D. L.; Searchinger, T. D.; Dumas, P.; Shen, Y. *Nature* **2015**, *9*, 1.

(2) https://minerals.usgs.gov, 2017.

(3) Jasuja, H.; Peterson, G. W.; Decoste, J. B.; Browe, M. A.; Walton, K. S. *Chem. Eng. Sci.* **2015**, *124*, 118.

(4) Peterson, G. W.; DeCoste, J. B.; Fatollahi-Fard, F.; Britt, D. K. *Ind. Eng. Chem. Res.* **2014**, *53* (2), 701.

(5) Britt, D.; Tranchemontagne, D.; Yaghi, O. M. *Proc. Natl. Acad. Sci. U. S. A.* **2008**, *105* (33), 11623.

(6) Qajar, A.; Peer, M.; Andalibi, M. R.; Rajagopalan, R.; Foley, H. C. *Microporous Mesoporous Mater.* **2015**, *218*, 15.

(7) Wang, K.; Do, D. D. *Langmuir* **1997**, *13*, 6226.

(8) Petit, C.; Bandosz, T. J. *Adv. Funct. Mater.* **2010**, *20* (1), 111.

(9) Van Humbeck, J. F.; McDonald, T. M.; Jing, X.; Wiers, B. M.; Zhu, G.; Long, J. R. *J. Am. Chem. Soc.* **2014**, *136* (6), 2432.

(10) Katz, M. J.; Howarth, A. J.; Moghadam, P. Z.; DeCoste, J. B.; Snurr, R. Q.; Hupp, J. T.; Farha, O. K. *Dalt. Trans.* **2016**, *45* (10), 4150.

(11) Grant Glover, T.; Peterson, G. W.; Schindler, B. J.; Britt, D.; Yaghi, O. *Chem. Eng. Sci.* **2011**, *66* (2), 163.

(12) Chen, Y.; Li, L.; Li, J.; Ouyang, K.; Yang, J. *J. Hazard. Mater.* **2016**, *306*, 340.

DOI: 10.1021/jacs.8b00313
J. Am. Chem. Soc. 2018, 140, 3461–3466

(13) Barin, G.; Peterson, G. W.; Crocellà, V.; Xu, J.; Colwell, K. A.; Nandy, A.; Reimer, J. A.; Bordiga, S.; Long, J. R. *Chem. Sci.* **2017**, *8*, 4399.
(14) Huberty, M. S.; Wagner, A. L.; McCormick, A.; Cussler, E. *AIChE J.* **2012**, *58* (11), 3526.
(15) Valyon, J.; Onyestyák, G.; Rees, L. V. C. *Langmuir* **2000**, *16* (3), 1331.
(16) Rieth, A. J.; Tulchinsky, Y.; Dincă, M. *J. Am. Chem. Soc.* **2016**, *138* (30), 9401.
(17) Rieth, A. J.; Yang, S.; Wang, E. N.; Dincă, M. *ACS Cent. Sci.* **2017**, *3* (6), 668.
(18) Tulchinsky, Y.; Hendon, C. H.; Lomachenko, K. A.; Borfecchia, E.; Melot, B. C.; Hudson, M. R.; Tarver, J. D.; Korzyński, M. D.; Stubbs, A. W.; Kagan, J. J.; Lamberti, C.; Brown, C. M.; Dincă, M. *J. Am. Chem. Soc.* **2017**, *139* (16), 5992.
(19) Deng, H.; Grunder, S.; Cordova, K. E.; Valente, C.; Furukawa, H.; Hmadeh, M.; Gándara, F.; Whalley, A. C.; Liu, Z.; Asahina, S.; Kazumori, H.; O'Keeffe, M.; Terasaki, O.; Stoddart, J. F.; Yaghi, O. M. *Science* **2012**, *336* (6084), 1018.
(20) Liao, P.-Q.; Li, X.-Y.; Bai, J.; He, C.-T.; Zhou, D.-D.; Zhang, W.-X.; Zhang, J.-P.; Chen, X.-M. *Chem. - Eur. J.* **2014**, *20* (36), 11303.
(21) Leistner, M.; Grählert, W.; Kaskel, S. *Chem. Ing. Tech.* **2013**, *85* (5), 747.
(22) Sandra, F.; Klein, N.; Leistner, M.; Lohe, M. R.; Benusch, M.; Woellner, M.; Grothe, J.; Kaskel, S. *Ind. Eng. Chem. Res.* **2015**, *54* (26), 6677.
(23) Oschatz, M.; Leistner, M.; Nickel, W.; Kaskel, S. *Langmuir* **2015**, *31* (13), 4040.
(24) Eigen, M. *Pure Appl. Chem.* **1963**, *6*, 97.
(25) Derouane, E. G.; Chang, C. D. *Microporous Mesoporous Mater.* **2000**, *35*−*36* (1387), 425.
(26) Park, S. S.; Tulchinsky, Y.; Dincă, M. *J. Am. Chem. Soc.* **2017**, *139* (38), 13260.
(27) Doonan, C. J.; Tranchemontagne, D. J.; Glover, T. G.; Hunt, J. R.; Yaghi, O. M. *Nat. Chem.* **2010**, *2* (3), 235.
(28) De Lange, M. F.; Verouden, K. J. F. M.; Vlugt, T. J. H.; Gascon, J.; Kapteijn, F. *Chem. Rev.* **2015**, *115* (22), 12205.
(29) Akimbekov, Z.; Navrotsky, A. *ChemPhysChem* **2016**, *17* (4), 468.
(30) Hughes, J. T.; Bennett, T. D.; Cheetham, A. K.; Navrotsky, A. *J. Am. Chem. Soc.* **2013**, *135* (2), 598.
(31) Choi, H. J.; Dincă, M.; Long, J. R. *J. Am. Chem. Soc.* **2008**, *130* (25), 7848.
(32) Choi, H. J.; Dincă, M.; Dailly, A.; Long, J. R. *Energy Environ. Sci.* **2010**, *3* (1), 117.
(33) Wade, C. R.; Corrales-Sanchez, T.; Narayan, T. C.; Dincă, M. *Energy Environ. Sci.* **2013**, *6* (7), 2172.
(34) Colombo, V.; Galli, S.; Choi, H. J.; Han, G. D.; Maspero, A.; Palmisano, G.; Masciocchi, N.; Long, J. R. *Chem. Sci.* **2011**, *2* (7), 1311.
(35) Dietzel, P. D. C.; Panella, B.; Hirscher, M.; Blom, R.; Fjellvåg, H. *Chem. Commun. (Cambridge, U. K.)* **2006**, *1* (9), 959.
(36) Kajiwara, T.; Higuchi, M.; Watanabe, D.; Higashimura, H.; Yamada, T.; Kitagawa, H. *Chem. - Eur. J.* **2014**, *20* (47), 15611.
(37) Férey, G.; Mellot-Draznieks, C.; Serre, C.; Millange, F.; Dutour, J.; Surblé, S.; Margiolaki, I. *Science* **2005**, *309* (5743), 2040.
(38) Kim, M.; Cahill, J. F.; Fei, H.; Prather, K. A.; Cohen, S. M. *J. Am. Chem. Soc.* **2012**, *134* (43), 18082.
(39) Kang, I. J.; Khan, N. A.; Haque, E.; Jhung, S. H. *Chem. - Eur. J.* **2011**, *17* (23), 6437.
(40) Jiao, Y.; Morelock, C. R.; Burtch, N. C.; Mounfield, W. P.; Hungerford, J. T.; Walton, K. S. *Ind. Eng. Chem. Res.* **2015**, *54* (49), 12408.
(41) Brozek, C. K.; Dincă, M. *Chem. Sci.* **2012**, *3* (6), 2110.
(42) Brozek, C. K.; Dinca, M. *Chem. Soc. Rev.* **2014**, *43* (16), 5456.
(43) Petit, C.; Mendoza, B.; Bandosz, T. J. *Langmuir* **2010**, *26* (19), 15302.
(44) Rezaei, F.; Webley, P. *Chem. Eng. Sci.* **2009**, *64* (24), 5182.
(45) Steckelmacher, W. *Rep. Prog. Phys.* **1986**, *49* (10), 1083.
(46) Barrett, E. P.; Joyner, L. G.; Halenda, P. P. *J. Am. Chem. Soc.* **1951**, *73* (1), 373.
(47) Kruk, M.; Jaroniec, M.; Sayari, A. *Langmuir* **1997**, *13* (23), 6267.

DOI: 10.1021/jacs.8b00313
J. Am. Chem. Soc. 2018, 140, 3461−3466